JOURNAL OF PROPULSION AND POWER
Vol. 15, No. 4, July–August 1999

Theoretical Analysis and Engineering Modeling of Flowfields in Clustered Module Plug Nozzles

Francesco Nasuti* and Marcello Onofri†
University of Rome "La Sapienza," 00184 Rome, Italy

The fluid dynamics of clustered module plug nozzles features nontrivial behaviors. The goal of this study is to point out some of the most important fluid dynamic aspects, to provide their detailed analysis by considering both the theoretical and the experimental points of view, and finally to develop engineering models capable of predicting the nozzle behavior and performance by easily applied mathematical relationships. Assessment of the quality of the engineering models has been performed by comparison with available experimental data.

Nomenclature

A = area
g = last characteristic line (Fig. 6)
M = Mach number
N = number of modules
$\boldsymbol{n}$ = unit vector normal to Π
PR = chamber of ambient pressure ratio
p = pressure
R = radial coordinate in the cylindrical frame of reference of the plug
r = radial coordinate in the cylindrical frame of reference of the module
$\boldsymbol{v}$ = velocity vector
v = velocity
x = axial coordinate in all frames of reference
y = coordinate in the direction normal to the axis and parallel to the plug surface
z = coordinate in the direction normal to the axis and to the plug surface
α = jet deviation angle at the module exit
β = angle of the last characteristic line g with respect to x
γ = ratio of specific heats
δ = module tilt angle
ε = area ratio (A/A_{th})
θ = circumferential coordinate in the cylindrical frame of reference of the module
μ = Mach angle
ν = Prandtl–Meyer function
Π = generic plane
Φ = plug exit angle
χ = flow angle on the plug surface
ψ = circumferential coordinate in the cylindrical frame of reference of the plug
ω = impingement angle of the flow on the plug surface

Subscripts

a = ambient
b = base
c = chamber
d = design
e = exit
eff = effective
eq = equivalent
j = jet
m = module
mb = module base
me = module exit
th = throat
tr = transition

Received 6 June 1998; revision received 21 January 1999; accepted for publication 8 February 1999.

*Postdoctoral Fellow, Dipartimento di Meccanica e Aeronautica, via Eudossiana 18. Member AIAA.
†Professor, Dipartimento di Meccanica e Aeronautica, via Eudossiana 18. Senior Member AIAA.

Introduction

THE analysis of rocket engines based on new-generation expansion devices having self-adapting capabilities has acquired growing interest due to the possible application of reusable launch vehicles. Indeed, in the design of the engines for future launchers, an important role is played by the performance of the expansion system working in a varying pressure environment. In this framework, many studies recently have been carried out, mainly devoted to the analysis of aerospike nozzles. Among them, an analysis of feasibility, followed by numerical and experimental work, has been promoted by the European Space Agency (ESA) in the framework of the Advanced Rocket Propulsion Technology (ARPT) program.[1] To date, a large set of experimental tests has been performed at the ONERA-R2Ch wind tunnel,[2] and the large amount of data has been analyzed by different teams in Europe having different tasks.

The experiments concern a clustered module plug nozzle (CMPN). It is an annular aerospike, whose primary (internal) expansion is achieved through a number of conventional bell nozzles (modules) circumferentially placed on the plug, rather than through a single annular primary nozzle surrounding the plug. The reasons for such a choice have been widely discussed in the literature (see, for instance, Refs. 3 and 4). It is important to note that this configuration allows easier manufacturing, lower thermal loads, easier cooling, higher thrust vector capability, and higher throttling.

In this paper some of the results obtained in the analysis of the general flow behavior around CMPN and in the development of engineering models for its prediction are discussed. Particular emphasis is given to the analysis of the consequences of module clustering for varying ambient pressure, as well as to the prediction of closed–open wake transition.

Theoretical Analysis

Two possible configurations of CMPN, whose design is discussed in Ref. 1, are considered. They display 12 and 24 modules (Fig. 1), respectively, with the gap between two neighboring modules vanishing in the latter configuration. The modules expand cold air for a pressure ratio $PR_m = 29$ and then exhaust over contoured plug shapes, truncated at different lengths (5, 20, and 40%, of the length of the ideal profile). The overall CMPN design pressure ratio is $PR_d = 200$. In all tests, different operating conditions have been obtained by varying p_a and keeping p_c constant.

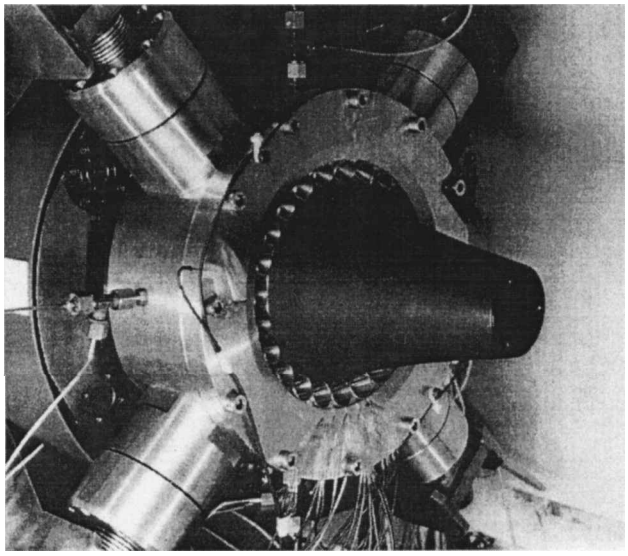

Fig. 1 CMPN configuration: 24 modules, 40% length.[2]

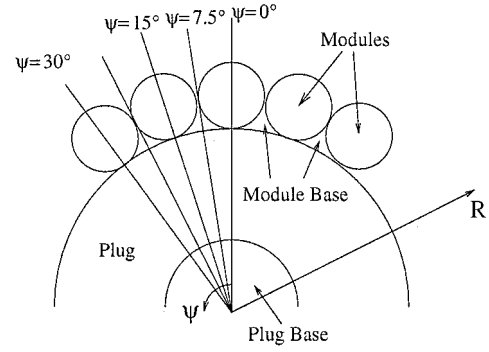

a) Schematic view

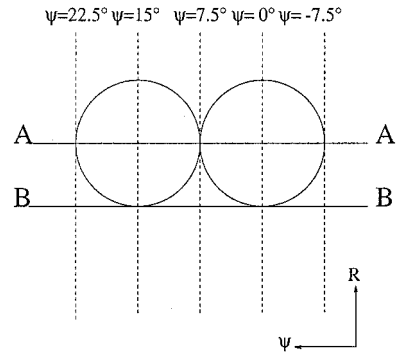

b) Conceptual scheme

Fig. 2 Cross section at the module exit.

Effects of Clustering of the Nozzle Modules

The analysis of the fluid dynamic behavior around CMPN can be performed by superimposing the strong three-dimensional effects related to the module clustering on the behavior of a plain axisymmetric plug nozzle.

The basic phenomena, largely discussed in the literature for annular and linear plug nozzles,[5–7] are perturbed in the case of CMPN by the interaction of the module jets. The interaction causes the formation of shocks, the location of which is important to predict, because it indicates the regions on the plug surface where maximum heat fluxes are expected. This interaction can be described by the following simple conceptual scheme.

Configuration with 24 Modules

The cross section at the modules' exit is shown in Fig. 2a, with the traces of the longitudinal symmetry planes at different ψ. This geometry can be simulated by the simplified scheme presented in Fig. 2b, with the plug surface transformed in a planar surface. Considerations about the flow structure can be done by analyzing the behavior of a planar jet in the two planes denoted as A–A and B–B in Fig. 2b.

Figure 3a shows the flow on the plane A–A. At the exit section, the nozzle jet has an angle, due to the specific geometry of the module divergent section. Because the distance between two neighboring modules is very small, the two jets must deviate their direction to accommodate each other. As a result, the flow structure emanating from the border zone between the two nozzles is characterized by a mixing layer and two shocks. The interaction between the two shocks coming from two neighboring border zones, which occurs on each module centerline, yields two other symmetrical shocks, with directions different than the previous ones.

Figure 3b shows the flow on the plane B–B, where the flow exhausts from the limited zone of tangency of the module exit cross section and the plug surface. In this case, to fill the gap between modules, an expansion takes place that brings down the flow pressure from the value at the module exit to the module base value, and that diverts the jet away from the module centerline, toward the neighboring modules. The consequent interaction of two neighboring exit jets takes place along the intermodular symmetry line, located at $\psi = \pm 7.5$ deg in Fig. 3b, and yields two symmetrical shocks directed toward the module axis, which interact with each other, like the shocks of section A–A. These shocks, and the further reflected waves generated by their subsequent interactions with the neighboring jets, affect the wall pressure trend along the plug in the radial planes containing the module axes ($\psi = 0, \pm 15$ deg). Therefore, the expected wall pressure behavior at $\psi = 0$ deg features the following sequence: An initial strong expansion is followed by a shock and by a second expansion. Farther downstream, the reflected waves are characterized by a lower intensity because of the superimposition of expansions and compressions and the increasing dissipation.

Note that the real three-dimensional configuration presents some other aspects, which can be assumed as a minor perturbation of this scheme. In particular, the plug regions close to the module exits are wet by the flow that falls, expanding from the circular module exit, and impinges on the plug surface. The trace of this flow on the plane B–B, approximated as a planar jet boundary in the scheme and indicated by the shaded zone in Fig. 3b, is a mixing layer between a recirculating flow in the base region and the main flow, which is also characterized by a shock generated by the exhaust gas dropping from the module exit.

The experimental data available from Ref. 1 confirm the foregoing conceptual scheme (Fig. 4a). In particular, the measured wall pressure at different *PR* shown in Fig. 4a indicates that there are two regions: In the first ($x < 60$ mm), there is no dependence on *PR*; whereas in the second ($x > 60$ mm), a dependence on *PR* occurs especially at the lower *PR*.

In the first region, an interesting feature to emphasize is that the effects of clustering dominate and make the flow independent of ambient pressure. Indeed, on the plane A–A, the angle of reflection of the shock depends only on the exit angle of the nozzle divergent section; whereas on the plane B–B, the location of the mixing layer is independent of *PR*, which has no practical consequence on the pressure value at the base of the modules. Thus, a dependence on the ambient pressure can only be expected when $PR < PR_m$, that is, when the overexpanded character of the modules makes their jets narrower than their exit section, establishing a connection between the module base and the ambient.

In the second region of Fig. 4a ($x > 60$ mm), the wall pressure follows the behavior of an ideal plug nozzle with annular throat: For p_{me} to adjust to p_a, an expansion fan emanates from the module lip, decreasing the wall pressure until it reaches the ambient value at a location on the plug wall that moves upstream as *PR* decreases. Downstream of this location, the concave plug shape generates compression waves that are then reflected as expansion waves when they hit the jet boundary. Thus, for the lower *PR*, Fig. 4a shows the

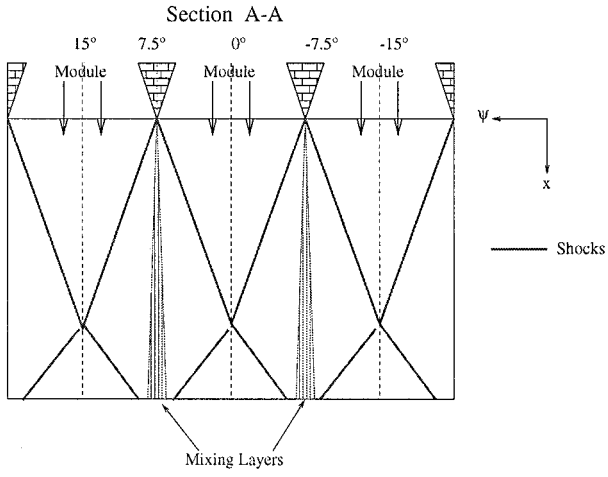

a) N = 24, plane A–A

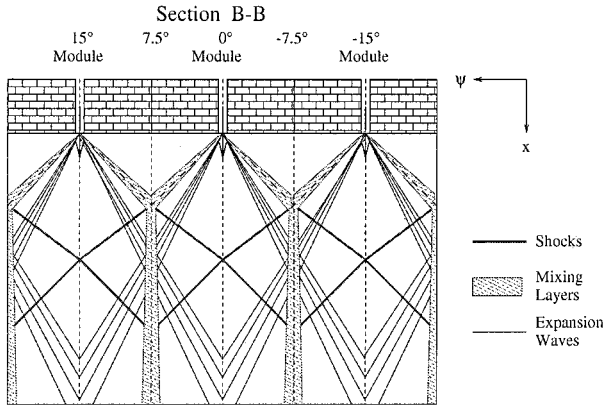

b) N = 24, plane B–B (plug surface)

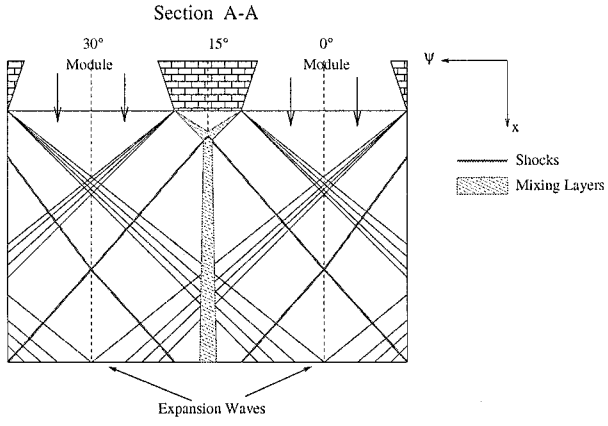

c) N = 12, plane A–A

Fig. 3 Conceptual scheme of the flow at the module exit.

well-known sequence of alternate compressions and expansions, described in detail in Ref. 6.

Configuration with 12 Modules

The same conceptual scheme of Fig. 2b can be implemented to simulate the general flow behavior for the configuration with 12 modules, separated by gaps. In particular, the section A–A can be represented as shown in Fig. 3c, whereas the section B–B can still be represented as shown in Fig. 3b, provided that the distance between the modules is rescaled: Module exits are now at $\psi = 0, \pm 30$ deg.

Note that all of the configurations with $N = 12$ and 24 have the same plug geometry, mass flow rate, and PR_m. Therefore, in comparison with the CMPN with $N = 24$, the CMPN with $N = 12$ features larger modules; thus, the major geometrical differences are: 1) the larger gap between two modules and 2) the larger distance between two neighboring modules' axes.

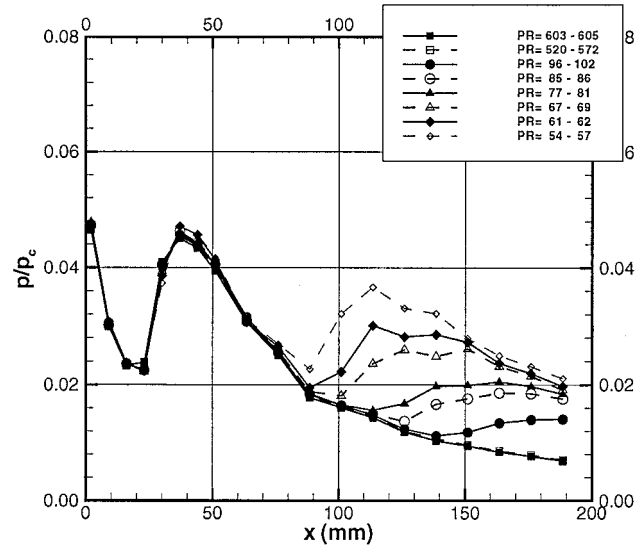

a) 24 Modules

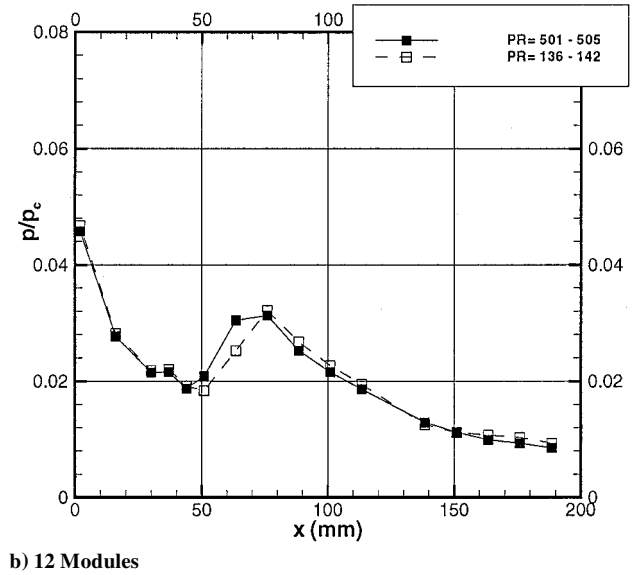

b) 12 Modules

Fig. 4 Wall pressure along the plug (40% length) at ψ = 0 deg, for different *PR* (Ref. 1).

Because of these differences, the module base pressure now depends on *PR*. The existence of a large gap between two neighboring modules allows a connection between the ambient and the recirculating flow in the module base region, contrary to the 24-modules configuration. Of course, if p_{mb} depends on *PR*, the slope of the mixing layers, the location where two neighboring jets interact, and the location where the resulting shocks cross each other will change as *PR* changes.

The experimental data confirm that in the first part of the plug the flow features a dependence on the pressure ratio. Figure 4b shows the wall-pressure behavior for two different *PR*, at $\psi = 0$ deg. The curves superimpose each other near the exit, but in the downstream region, at $x = 50$–75 mm, the shock takes place in locations dependent on the specific *PR*.

Comparison of Figs. 4b and 4a also shows that the shock is located downstream in the case of $N = 12$ because of the longer paths the expansion waves and shocks have to run before interacting with each other.

Opening and Closure of the Wake

As is well known, understanding the mechanism of transition from an open to a closed wake in the region behind the truncated base is very important for applications of plug nozzles. Indeed, its knowledge allows the prediction of the transition, from negative to

positive, of the contribution of the plug base pressure to the nozzle thrust and, consequently, of the nozzle performance along the flight trajectory.

Many experimental and theoretical studies have been performed on the flow evolution behind truncated plugs or more generally behind backward-facing steps. Among them, note the analyses of plug nozzles performed by Sule and Mueller,[8] the theoretical considerations about the flow rotation in base regions performed by Weiss and Weinbaum,[9] and finally the large number of recent numerical analyses on the backward-facing step problem.[10–12]

From the many visualizations reported in these studies it can be noted that there is no clear definition of the transition point between the two wake structures. Therefore, it is useful to establish a definition based on a practical aspect, considering the pressure value that takes place on the base: Open wake is the flow structure featuring a base pressure depending on the ambient pressure; and closed wake is the flow structure featuring a base pressure independent of the ambient pressure. For example, the base pressure values p_b in different sampling points are shown in the lowest part of Fig. 5 along with the ambient pressure p_a and the wall pressure at the plug lip, p_B. Figure 5 shows that p_b depends on PR in the range of low values, whereas it becomes constant for higher PR. Therefore, according to the present definition, the transition of the wake structure occurs at $PR \simeq 168$.

It is important to note that, although it is possible to find a wide number of studies on the base pressure prediction, the transition from open to closed wake has not been analyzed in the same depth. The following analysis of the flow behavior should provide greater insight into the main aspects of the wake structure transition.

A schematic view of the flow structure is shown in Fig. 6, where the three-dimensional effects due to clustering have been neglected, as well as the reflected waves possibly generated on the plug surface. Moreover, the mutual interaction among the waves shown in Fig. 6 is considered as a second-order effect, and therefore, it is neglected.

Independently of the wake shape, of the trailing shock position, and of the possible definition of a wake neck (often introduced to evaluate base pressure), it is possible to say that the wake is independent of p_a if the last characteristic wave g of the Prandtl–Meyer expansion centered in D impinges on the wake downstream of the reattachment point E. This is clear when F, the foot of g, is placed downstream of the sonic point S. In this case, any change in the ambient pressure would only move g inside a supersonic flow, without changing anything in the flow upstream. On the other hand, when F lies between E and S, only a slight effect on p_b is expected, whereas the position of g will certainly affect p_b when it impinges directly on the separated region. Therefore, for increasing p_a, the ambient pressure effect carried by the position of the line g begins to affect significantly the base region only when F reaches the reattachment region around E.

Understanding the closed–open wake transition phenomenon allows the development of suitable engineering models as it will be described in the following section.

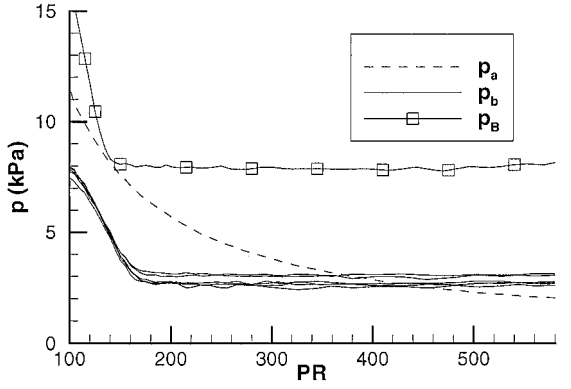

Fig. 5 Measured base pressure and plug exit pressure as a function of *PR*: 24 modules.[1]

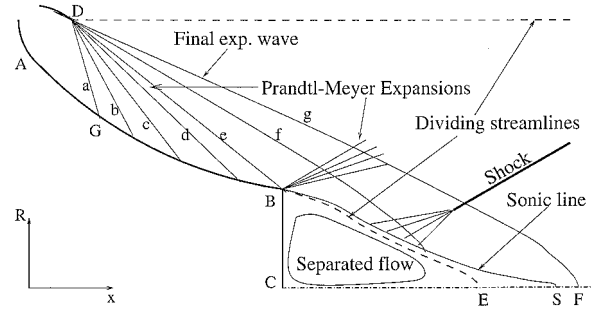

Fig. 6 Schematic view of the plug nozzle flow structure; closed wake operation.

Engineering Models

During the present study, engineering models were developed, aimed at determining nozzle performance for practical purposes. Two analytical models are illustrated, which allow the prediction of the general flow structure around the plug and the pressure ratio at the transition from closed to open wake operation.

Analytical Model of the Interaction Between the Module Exhaust Jet and the Plug Surface

A simple analytical model of the flow behavior in the plug region close to module exits has been developed by assuming as a general framework the conceptual scheme of Fig. 2b as well as considering the major three-dimensional effects.

Therefore, as first simplifying assumptions, the actual modules are replaced by cylindrical modules and the actual plug surface by a plane surface, so that each module is assumed to lie on a plane plug surface. A second simplification is to consider uniform axial flow in the cross section of the module exit. The flow values considered are the average module exit values.

As a further assumption, needed to implement the model, a uniform pressure value in the base region between the module jets is considered. Once this pressure is known, the Prandtl–Meyer expansion relations provide the angle α that is the change of direction of the flow because of the expansion from p_{me} to p_{mb} ($< p_{me}$). The same relations also allow the computation of the Mach number M_j of the expanded jet.

In the region close to the module exit, the exhaust jet can be assumed as bounded by a conical surface having cone half-angle equal to α. The conical surface interacting with the plug surface is shown in Fig. 7. The equation of the conical jet boundary can be easily written in a coordinate system with origin in the intersection between the module axis and the module exit section as

$$y^2 + z^2 = (x \tan\alpha + r_m)^2 \tag{1}$$

where r_m is the module radius.

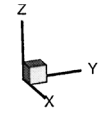

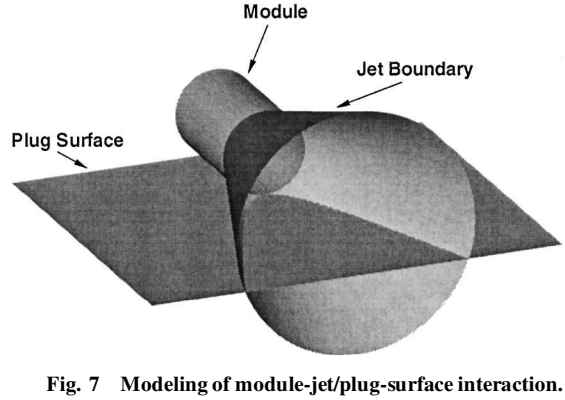

Fig. 7 Modeling of module-jet/plug-surface interaction.

The conical jet of Eq. (1) is not free, but it intersects the plug surface. In the model the plug surface is a planar surface described by

$$z = -r_m \tag{2}$$

The intersection line is, therefore, a hyperbola of the equation

$$y^2 = (x \tan\alpha + r_m)^2 - r_m^2 \tag{3}$$

This hyperbola represents the boundary on the plug surface of the area wetted by the jet. Moreover, it is a shock line because the jet flow exhausting from the module impinges on the surface at an angle. A view of this curve on the plug surface is shown in Fig. 8.

The strength of the shock due to the impingement of the supersonic jet on the plug surface can be evaluated as follows. Let A be a generic point along the hyperbolic shock (Fig. 8), shown in Fig. 9 in a cross section normal to the plug surface and to the module axis, passing in A ($x = x_A$). The velocity vector in A, $\boldsymbol{v} = (v\cos\alpha,\ v\sin\alpha\cos\theta,\ v\sin\alpha\sin\theta)$, before interacting with the plug surface, lies on the jet boundary surface and, therefore, because of the conical symmetry, lies along the cone generatrix passing in A. Thus, it can be considered a plane Π including $\boldsymbol{v}$ and perpendicular to the plug surface. To identify the plane Π, whose normal $\boldsymbol{n} = (n_x, n_y, 0)$ lies on the plug surface, the two vectors $\boldsymbol{v}$ and $\boldsymbol{n}$ must be perpendicular to each other, and, therefore,

$$n_x \cos\alpha + n_y \sin\alpha\cos\theta = 0 \tag{4}$$

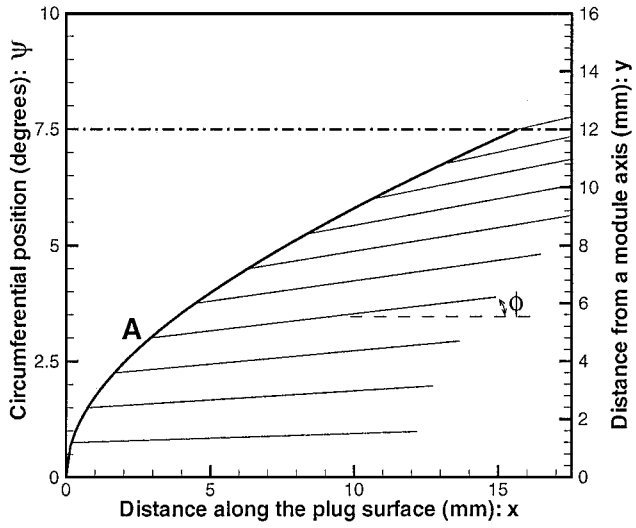

Fig. 8 Hyperbolic shape of the trace of the jet boundary on the plug surface and straight lines indicating the flow direction; $N = 24$.

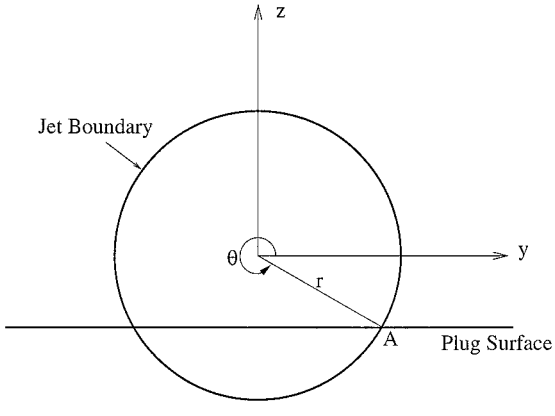

Fig. 9 Cross section normal to the plug surface at a distance x_A from the module exit.

As a consequence, the plane Π passing in the generic point $A \equiv (x_A, y_A, -r_m)$ has the equation

$$y = y_A + \tan\alpha\cos\theta(x - x_A) \tag{5}$$

The intersection of Π with the plug surface is shown in Fig. 8 by the diverging line emanating from the hyperbola in A. It is possible to see that this line, and then the velocity vector, shows an angle χ with the axial direction, which increases as the point A is moved away from the module axis. It can be easily seen that χ is given by

$$\tan\chi = \tan\alpha\cos\theta \tag{6}$$

The next assumption is that the jet/surface interaction takes place in the plane Π. In this case, the supersonic jet must deviate of an angle ω that can be computed as

$$\sin\omega = v_z / v = \sin\alpha\sin\theta \tag{7}$$

From ω and M_j and the use of the oblique shock relations, it is possible to compute the conditions behind the shock and then to obtain an easy evaluation of the location and strength of pressure and temperature maxima on the plug surface. In particular, the shock strength depends only on the deflection angle ω because the upstream Mach number is constant and equal to M_j. Therefore, α being constant, ω has a maximum when $\theta = \pm 90$ deg, that is, when $y = 0$. Nevertheless, this maximum strength value cannot be reached because there is no expansion and, therefore, no shock at $y = 0$. On the other hand, the minimum strength is at the symmetry line between modules, where there is also the maximum in the flow deviation from the module axis. Nevertheless, at this symmetry line, the pressure on the plug surface reaches its higher values. The reason is that a reflected shock takes place on the plug surface to turn the flow back in the axial direction at the symmetry line, whose strength depends on χ and on the Mach number M_χ behind the first impingement shock. Note that both M_χ and χ increase moving away from the module centerline. In conclusion, the maximum shock intensity, and consequently pressure and temperature behind it, occurs at the intermodular symmetry lines and increases as the distance between two neighboring modules increases.

The simplified model, applied to the CMPN configurations by using the experimental data[1] for p_{mb}, provides the results shown in Fig. 10, where, besides the hyperbolic shocks, straight shocks have been also drawn as an approximate trace of their reflection at the intermodular symmetry line. Several experimental data are displayed along with the shocks computed by the model. The first set of data[1] is denoted by squares and horizontal error bars, which indicate the regions where pressure maxima are located. Error bars are used because the finite number of pressure taps leaves an uncertainty of the exact position of the maxima. The second data set,[1] available for the 24-module configuration only, is denoted by a dashed line and vertical error bars, and shows the line where the surface streamlines abruptly change direction in oil visualization images (Fig. 11). Superimposed are the numerical results obtained in Ref. 13 by a long three-dimensional calculation: The horizontal error bars are related to the existence of a plateau of the values at that location.

Figure 10 shows that there is a reasonable agreement between analytical prediction and experimental data. The wall pressure measured by the pressure taps placed along the plug surface shows compressions zones rather than shocks (see Figs. 4a and 4b); however, the comparison of the pressure maxima with the oil visualization indicates that shock waves occur at the end of the compression zones. The experimental data show good agreement with the numerical results of Ref. 13, whereas the present model predicts a slight displacement of both the slope of the reflected shock and the reflection point because of its inviscid approximation. Indeed, Fig. 11 shows a significant mixing layer thickness, whose effect is to move upstream the reflection point of the shock.

It is important to stress that the analytical model yields a good prediction of the hyperbolic shock line, as shown by comparison with the numerical results and with the experimental data available for both $N = 24$ and 12. In particular, in the case of 12 modules

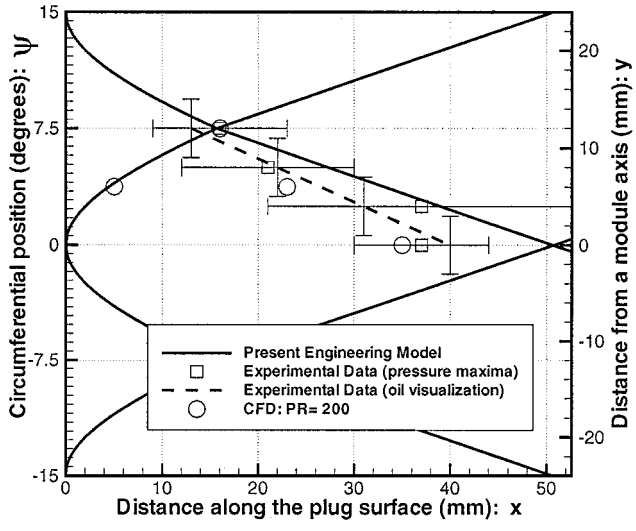

a) 24 Modules

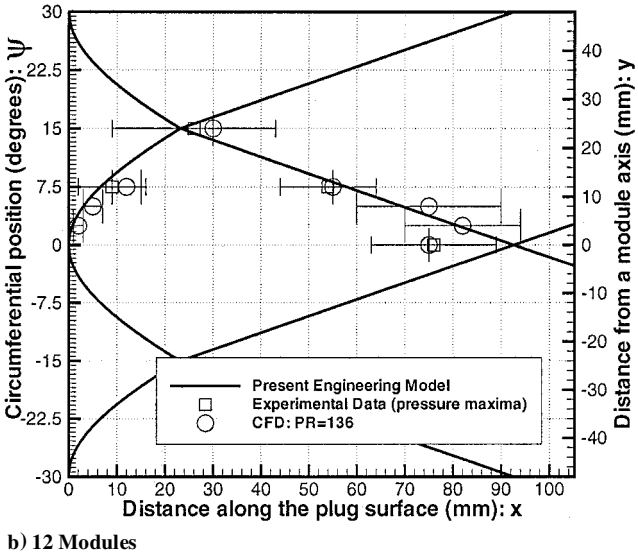

b) 12 Modules

Fig. 10 Analytical model of the shock traces on the plug surface compared with experimental[1] and numerical[13] data.

(Fig. 10b), the greater extension in y (circumferential) direction of the hyperbola, allows having in the same distance a larger amount of data with which to compare. The analytical model also provides a good prediction of the location where the jets cross each other at the intermodular symmetry line, as the comparison with experimental and numerical data shows. On the contrary, some slight discrepancies occur in the quantitative prediction of the reflected shock. Besides the shifting due to viscous effects, there is also a slight discrepancy on its slope that can be explained as an effect of the interaction between the shock and the expansion that the flow experiences moving from the module centerline toward the symmetry line between modules. Moreover, the neglect of other three-dimensional effects in the simulation model could have affected the evaluation of the reflected shock position and slope.

Analytical Model of Closed–Open Wake Transition

Basic Model

An engineering model has been developed to predict the pressure ratio PR_{tr} at which the closed–open wake transition occurs. This model is based on the schematic view of the flow structure shown in Fig. 6 and discussed in the preceding sections. Note that only few attempts to model PR_{tr} can be found in the literature,[14] and unfortunately their application leads to predictions quite far from the present experimental data.

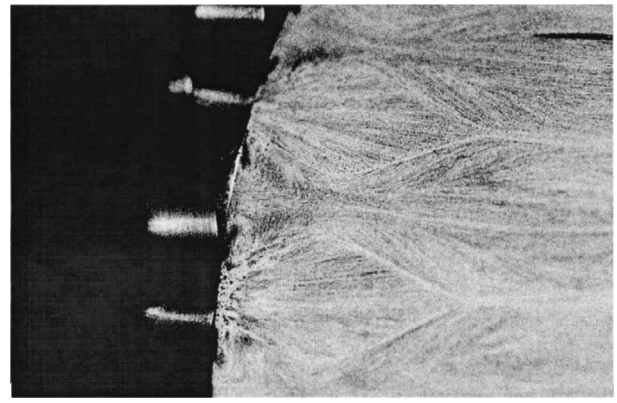

Fig. 11 Oil visualization of the flow on the plug surface at the module exit.[1]

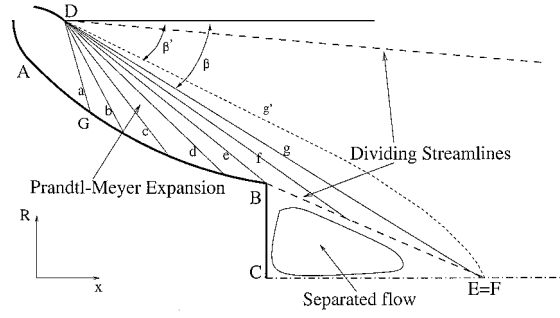

Fig. 12 Schematic of the simplified model of characteristic lines at closed–open wake transition.

The preceding theoretical analysis has shown that transition should occur when the final expansion wave g, emanating from the lip of the module exit section, impinges in the neighborhood of the reattachment point (E in Fig. 6). Therefore, a possible approach to evaluate PR_{tr} may be based on the analysis of the path of g for varying PR. Moreover, the assumption of axisymmetric flow can be made because the effects of dissymmetries due to the clustering on the base region can be reasonably neglected.

To evaluate the point F where the wave g impinges on the nozzle axis, note that the characteristic lines cannot be approximated by straight lines because they are curved by the axisymmetric effect, especially near the symmetry axis. To help visualize that, Fig. 12 shows an enhanced effect of the flow axisymmetry on the curvature of a characteristic line. Compared to the straight line g, the actual line g' corresponds to the larger expansion indicated by the angle β'. Therefore, for an assigned PR, the classic Prandtl–Meyer expansion relations can be used to compute the angle β'. Then the corrected angle $\beta = \beta' + \Delta\beta$ allows drawing the straight line that determines F. The analysis of both ARPT and literature data[1,4,15] shows that in these cases a constant value $\Delta\beta = 5$ deg can be assumed. At this point a model to evaluate PR_{tr} can be easily made available. Once the position of the point E, i.e., the maximum axial extension of the separated bubble CE, is known, it is possible to evaluate the corresponding β' and, thus, PR_{tr}, by inverting

$$\beta' = \mu(M_{tr}, \gamma) - \nu(M_{tr}, \gamma) + \nu(M_e, \gamma) + \delta \tag{8}$$

$$M_{tr} = \left\{[2/(\gamma - 1)]\left(PR_{tr}^{(\gamma-1)/\gamma} - 1\right)\right\}^{0.5}$$

There are different possible ways to evaluate CE. Following Refs. 16 and 17, the bubble extension of a supersonic backward-facing step seems to be independent of the approaching flow Mach number[16] for $M > 2$ and its value[17] such that CE $\simeq 2.65 \times$ BC. The results obtained for the present and some literature CMPN configurations by using this value of CE are reported on the fourth column of Table 1. These results have been obtained by introducing an equivalent external radius R_{eq} to evaluate the position of point D

Table 1 Prediction of PR_{tr}: basic model

N	Length, %	Φ, deg	PR_{tr}[a]	PR_{tr}[b]	PR_{tr}[c]	Data
24	40.0	10	171	166	**168**	Reference 1
24	20.0	14	131	117	**112**	Reference 1
24	5.0	20	117	78	**73**	Reference 1
12	40.0	10	160	155	**165**	Reference 1
12	20.0	14	121	108	**108**	Reference 1
12	5.0	20	108	72	**77**	Reference 1
24	9.4	13	148	129	**130**	Reference 15
24	0.0	18	137	96	**100**	Reference 15
12	20.0	18	46	38	**40**	Reference 4

[a]Prediction (R_{eq}). [b]Prediction [R_{eq} and (10)]. [c]Experimental data.

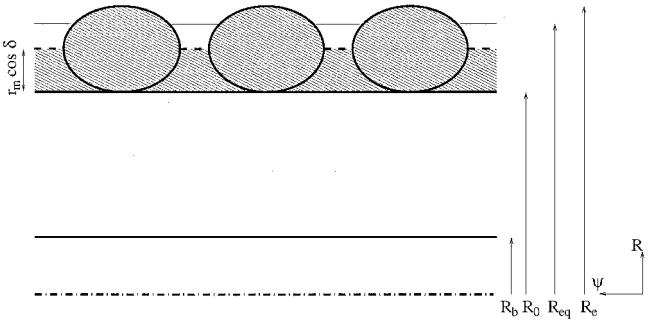

a) Equivalent external radius R_{eq}

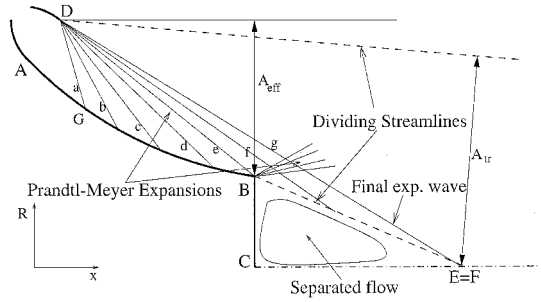

b) Effective exhaust area A_{eff}

Fig. 13 Definition of useful quantities.

(Fig. 12). The reason for the introduction of R_{eq} is that the exhaust jet has to fill the region between modules, and thus, the extension of the jet is no longer equivalent to an annular primary nozzle of external radius R_e (Fig. 13a), but to an annular primary nozzle of smaller external radius R_{eq}. This concept, introduced by Fick and Schmucker,[18] has been used here with a slightly different expression for the definition of R_{eq}. The equivalent annular primary nozzle has been considered as that whose exhaust area is equivalent to the filled area in Fig. 13a, obtained as the sum of the modules' section area and of half the gaps' area. By this definition, R_{eq} can be computed as

$$R_{eq}^2 = (R_e - r_m \cos\delta)^2 + 0.5 N r_m^2 \cos\delta \tag{9}$$

where $r_m \cos\delta$ is the projection of the module radius in the plane normal to the plug axis.

The comparison with experimental data relevant to nine different tests (sixth column of Table 1) shows good agreement only for the longer plugs, even if the actual large error bar is considered. In particular, note that the shorter the plug is the higher the discrepancy is. This is not surprising because the shorter the plug is, the larger the plug exit angle is, and the farther from a backward-facing step the wake behaves. Therefore, to evaluate CE, a correction should be introduced to the foregoing ratio CE/BC = 2.65 to consider the departure from a backward-facing step case. The most effective parameter to achieve this correction, rather than simply the plug length, is the plug exit angle Φ, that is, the wall slope at B with respect to the axis, as the comparison between the ARPT and literature tests suggest (Table 1). For instance, the 9.4% plug of Ref. 15, although shorter, features an exit angle smaller than the 20% plug of Ref. 1, and, therefore, is closer to a cylinder.

This analysis suggests to find a correlation expressing the ratio CE/BC as a function of Φ, by the assuming of the value CE/BC = 2.65 when $\Phi = 0$ deg according to Ref. 17. A correlation of the available data for $N = 24$ is given by

$$\mathrm{CE/BC} = 2.65 - 0.00144\Phi^2 \tag{10}$$

The results obtained with this correction improve significantly the agreement with the experimental data, as shown in the fifth column of Table 1.

Simpler Model

The basic model can be further simplified on the basis of the following considerations. It has been shown that the transition of the wake structure takes place at the pressure ratio $PR_{tr} \simeq p_c / p_E$. Assuming a one-dimensional flow simulation, the flow conditions at PR_{tr} are such that a uniform flow, with an angle in respect to the axis, exhausts at $p = p_E$ through the area A_{tr} (Fig. 13b).

On the basis of this scheme, the value PR_{tr} could be easily computed as a function of the area ratio between A_{tr} and A_{th}, the total nozzle throat area given by the sum of the module throat areas. Unfortunately, the evaluation of A_{tr} is not straightforward, because it is a function of the angle of the exhaust jet and of the position of the point E.

Nevertheless, the analysis of the Fig. 13b, as well as of the experimental data, shows that the effective exhaust area denoted as A_{eff} in Fig. 13b is nearly equivalent to the actual exhaust area A_{tr}. This effective area is defined as the annular section between the exhaust radius R_{eq} and the base radius, and therefore is very easily computed as

$$A_{eff} = \pi\left(R_{eq}^2 - R_b^2\right) \tag{11}$$

The introduction of the effective exhaust area and of the corresponding effective area ratio $\varepsilon_{eff} = A_{eff}/A_{th}$ provides the fast prediction $PR_{tr} \simeq PR_{eff}$, where PR_{eff} is obtained by the simple inversion of the function

$$\varepsilon_{eff} = \left[\frac{\gamma-1}{2}\left(\frac{2}{\gamma+1}\right)^{(\gamma+1)/(\gamma-1)} PR_{eff}^{(\gamma+1)/\gamma}\left(PR_{eff}^{(\gamma-1)/\gamma} - 1\right)^{-1}\right]^{0.5} \tag{12}$$

In fact, even if the prediction is less precise than the one provided by the basic model, it can be used for a first and quick evaluation. In particular, Table 2 shows that the isentropic expansion ratio PR_{eff} computed by using ε_{eff} provides a good compromise between simplicity and accuracy (in the range of 15% of error) in the prediction of the actual transition pressure ratio for the plug truncation lengths longer than 20%. Unfortunately, this simpler model fails to predict the transition for the shortest plugs (errors up to 50%).

Table 2 Prediction of PR_{tr}: simpler model

N	Length, %	PR_{eff}[a]	PR_{tr}[b]	Data
24	40.0	147	**168**	Reference 1
24	20.0	108	**112**	Reference 1
24	5.0	56	**73**	Reference 1
12	40.0	168	**165**	Reference 1
12	20.0	127	**108**	Reference 1
12	5.0	71	**77**	Reference 1
24	9.4	93	**130**	Reference 15
24	0.0	49	**100**	Reference 15
12	20.0	39	**40**	Reference 4

[a]Prediction (R_{eq}). [b]Experimental data.

Conclusions

The flow evolution around CMPN has been first analyzed on a theoretical basis to achieve a general interpretation of the flowfield behavior, which has been confirmed by comparisons with the data provided by experimental tests. Then engineering models have been developed, based on physical interpretations of the flow behavior and on correlations of the existing data. These models have been validated, showing in some cases excellent prediction capabilities. To appreciate the importance of these models, it should be considered that these indications otherwise could be obtained as the result of very complex and time-consuming numerical calculations. The main conclusions are summarized in the following.

Effect of Clustered Modules

A qualitative discussion of the effects of the interaction of the module jets on the flow behavior on the plug surface has been presented. The experimental data confirm the theoretical expectations of the flow behavior. A dependence on *PR* occurs when there is a significant gap between the modules. In these cases, the traces of the shocks downstream the module exit depend on the *PR* considered.

Wake Structure Estimation

A definition and an interpretation of the mechanism that drives the transition from closed to open wake have been proposed, yielding good theoretical explanation of the experimental results.

Engineering Models

Models capable of providing easy but reliable predictions of the flow behavior have been developed. In particular, on the basis of the present physical interpretation of the phenomena and on the existing correlation of the experimental data, two engineering models have been developed for the prediction of 1) the flow structure on the plug surface at the module exit and 2) the closed–open wake transition.

The first model has shown the capability to predict the general characteristics of the flow behavior on the plug, including the location of the shock interactions and, thus, of the hot spot regions. It has been validated by comparisons with the experimental data, which show a good agreement.

The second model has been validated by comparisons with the available data from experimental tests and has shown excellent agreement between analytical predictions and measured values of the pressure ratio at which the transition occurs. A simpler version has been also presented that can be used for a preliminary evaluation of PR_{tr}.

Acknowledgments

The present study is part of the Advanced Rocket Propulsion Technology program financed by the European Space Agency and coordinated by SEP-Division de Snecma. The experimental tests mentioned in the paper were performed by ONERA at the R2Ch test facility. The data have been analyzed by the teams involved in the Advanced Rocket Propulsion Technology research program: Volvo Aero Corporation; DLR, German Aerospace Research Establishment, Lampoldshausen, Germany; Daimler–Benz Aerospace; and University of Rome "La Sapienza." The authors want to acknowledge the support of M. De Sio in handling the large amount of data and for useful discussions.

References

[1] "ARPT—Advanced Rocket Propulsion Technology Program: Phase 3, Final Report," ESA/European Space Research and Technology Center, TR ESTEC/Contract 12219/96/NL/FG—Phase 3.1, Noordwijk, The Netherlands, April 1998.

[2] Hallard, R., and Merienne, M., "Aerospike Nozzle Tests," *Proceedings of the 3rd Symposium on Aerothermodynamics for Space Vehicles,* ESA/European Space Research and Technology Center, SP-426, Noordwijk, The Netherlands, 1998, pp. 387–394.

[3] Rommel, T., Hagemann, G., Schley, C. A., Krülle, G., and Manski, D., "Plug Nozzle Flowfield Analysis," *Journal of Propulsion and Power*, Vol. 13, No. 5, 1997, pp. 629–634; also AIAA Paper 95-2784, July 1995.

[4] Tomita, T., Takahashi, M., and Tamura, T., "Flow Field of Clustered Plug Nozzles," AIAA Paper 97-3219, July 1997.

[5] O'Leary, R., and Beck, J., "Nozzle Design," *Threshold,* No. 8, Rockwell International Co., Canoga Park, CA, Spring 1992, pp. 34–43.

[6] Nasuti, F., and Onofri, M., "Methodology to Solve Flowfields of Plug Nozzles for Future Launchers," *Journal of Propulsion and Power*, Vol. 14, No. 3, 1998; also AIAA Paper 97-2941, July 1997.

[7] Immich, H., Nasuti, F., Onofri, M., and Caporicci, M., "Experimental and Numerical Analysis of Linear Plug Nozzles," AIAA Paper 98-1603, April 1998.

[8] Sule, W., and Mueller, T., "Annular Truncated Plug Nozzle Flowfield and Base Pressure Characteristics," *Journal of Spacecraft*, Vol. 10, No. 11, 1973, pp. 689–695.

[9] Weiss, R., and Weinbaum, S., "Hypersonic Boundary-Layer Separation and the Base Flow Problem," *AIAA Journal*, Vol. 4, No. 8, 1966, pp. 1321–1330.

[10] Broglia, R., Di Mascio, A., Favini, B., Nasuti, F., Onofri, M., and Paciorri, R., "CFD Analysis of Axisymmetric Plug Nozzle Flowfields," ESA/European Space Research and Technology Center, TR ESTEC/Contract 12019/96/NL/FG, Technology and Research Projects, Noordwijk, The Netherlands, July 1997.

[11] Loth, E., Kailasanath, K., and Lockner, R., "Supersonic Flow over an Axisymmetric Backward-Facing Step," *Journal of Spacecraft and Rockets*, Vol. 29, No. 3, 1992, pp. 352–359.

[12] Tucker, P. K., and Shyy, W., "A Numerical Analysis of Supersonic Flow over an Axisymmetric Afterbody," AIAA Paper 93-2347, June 1993.

[13] Hagemann, G., "Clustered Plug Nozzle Flowfield Simulations—ARPT 4100/4200/2460," DLR, German Aerospace Research Establishment, TR DLR-IB 645-98/1, Lampoldshausen, Germany, Feb. 1998.

[14] Fick, M., "Performance Modeling and Systems Aspects of Plug Cluster Nozzles," AIAA Paper 98-3525, July 1998.

[15] Hendershot, K., Sergeant, R., and Wilson, H., "A New Approach for Evaluating the Performance and Base Environment Characteristics of Nonconventional Rocket Propulsion Systems," AIAA Paper 67-256, Feb. 1967.

[16] Chang, P., *Separation of Flow,* Pergamon, Oxford, 1970, pp. 541–554.

[17] Herrin, J., and Dutton, J., "Supersonic Base Flow Experiments in the Near Wake of a Cylindrical Afterbody," *AIAA Journal*, Vol. 32, No. 1, 1994, pp. 77–83.

[18] Fick, M., and Schmucker, R., "Remarks on Plug Cluster Nozzles," AIAA Paper 95-2694, July 1995.